



Cite this: *Dalton Trans.*, 2017, **46**, 8091

Near-infrared-emitting heteroleptic cationic iridium complexes derived from 2,3-diphenylbenzo[g]quinoxaline as *in vitro* theranostic photodynamic therapy agents†

Li Wang,^a Huimin Yin,^b Peng Cui,^{a,c} Marc Hetu,^b Chengzhe Wang,^a Susan Monro,^b Richard D. Schaller,^d Colin G. Cameron,^e Bingqing Liu,^a Svetlana Kilina,^{ID a} Sherri A. McFarland^{ID *b,e} and Wenfang Sun^{ID *a}

Five heteroleptic cationic iridium complexes with a π -expansive cyclometalating 2,3-diphenylbenzo[g]quinoxaline (dpbq) ligand (C[^]N ligand) and different diimine ligands (N[^]N ligands) (*i.e.* 2,2'-bipyridine (bpy, **1**), phenanthroline (phen, **2**), 2-(2-pyridinyl)quinoline (pqu, **3**), 2,2'-bisquinoline (bqu, **4**), and 2-(quinolin-2-yl)quinoxaline (quqo, **5**)) were synthesized and characterized. The lowest-energy singlet electronic transitions (S_1 states) were mainly dpbq ligand-centred 1 ILCT (intraligand charge transfer)/ 1 MLCT (metal to ligand charge transfer) transitions mixed with some $^1\pi,\pi^*$ transitions for complexes **1–4** with increased contributions from 1 LLCT (ligand to ligand charge transfer) in **3** and **4**. For complex **5**, the S_1 state was switched to the 1 LLCT/ 1 MLCT transitions. All five complexes displayed weak near-infrared (NIR) phosphorescence, with maximal emission output spanning 700–1400 nm and quantum yields being on the order of 10^{-3} . The triplet state absorptions of **1–4** all resembled that of the $[\text{Ir}(\text{dpbq})_2\text{Cl}]_2$ dimer with lifetimes of *ca.* 400 ns, while the TA spectrum of **5** possessed the characteristics of both the quqo ligand and the $[\text{Ir}(\text{dpbq})_2\text{Cl}]_2$ dimer with a bi-exponential decay of *ca.* 5 μs and 400 ns. While the photophysics of these complexes differ slightly, their theranostic photodynamic therapy (PDT) effects varied drastically. All of the complexes were biologically active toward melanoma cells. Complexes **2** and **3** were the most cytotoxic, with 230–340 nM activity and selectivity factors for melanoma cells over normal skin fibroblasts of 34 to 40 fold. Complexes **2**, **3**, and **5** became very potent cytotoxins with light activation, with EC_{50} values as low as 12–18 nM. This potent nanomolar light-triggered activity combined with a lower dark toxicity resulted in **5** having a phototherapeutic index (PI) margin of almost 275. The bpy coligand led to the least amount of dark toxicity of **1**, while phen and pqu produced cytotoxic but selective complexes **2** and **3**. The quqo coligand produced the most potent complex **5** for *in vitro* PDT, both in terms of photocytotoxicity and PI. All $\text{Ir}(\text{III})$ complexes exhibited very bright NIR phosphorescence in melanoma cells. The wide range of cytotoxicity and photocytotoxicity effects within a relatively small class of complexes highlights the importance of the identity of the coligand in the biological activity of the π -expansive biscyclometalated $\text{Ir}(\text{III})$ complexes, and their bright NIR emission in live cells demonstrates their potential as theranostic PDT agents.

Received 13th March 2017,
Accepted 19th May 2017

DOI: 10.1039/c7dt00913e

rscl.li/dalton

^aDepartment of Chemistry and Biochemistry, North Dakota State University, Fargo, North Dakota 58108-6050, USA. E-mail: Wenfang.sun@ndsu.edu

^bDepartment of Chemistry, Acadia University, 6 University Avenue, Wolfville, NS B4P 2R6, Canada

^cMaterials and Nanotechnology Program, North Dakota State University, Fargo, North Dakota 58105, USA

^dCenter for Nanoscale Materials, Argonne National Laboratory, Argonne, IL 60439, USA

^eDepartment of Chemistry and Biochemistry, University of North Carolina at Greensboro, 310 McIver Street, Greensboro, NC 27402-6170, USA

† Electronic supplementary information (ESI) available: Experimental details for the photobiological activity studies, NMR and mass spectra, solvent dependent UV-vis absorption spectra, comparison of the experimental and calculated UV-vis absorption spectra, natural transition orbitals (NTOs), time-resolved nanosecond TA spectra, *in vitro* dose-response curves for complexes **1–5** in CCD-1064Sk normal fibroblasts, and the comparison of *in vitro* dose-response curves for complexes **1–5** in SK-MEL-28 cells. See DOI: 10.1039/c7dt00913e

Introduction

Photodynamic therapy (PDT) is an underexploited anticancer modality that works by destroying tumors and tumor vasculature and invoking an immune response.^{1,2} Historically, organic porphyrin-related compounds have been employed as photosensitizers (PSs) for PDT based on a mechanism that involves cytotoxic singlet oxygen ($^1\text{O}_2$) sensitized by the PS in oxygenated environments.³ More recently, metal complexes based on Ru and Os have been explored as PSs,^{4–8} and one Ru compound, TLD1433, is currently in a clinical trial for treating bladder cancer with PDT (ClinicalTrials.gov Identifier: NCT03053635).⁹ The hope is that the metal complexes will overcome some of the limitations of the organic PSs that have hindered the development of PDT, namely, oxygen dependence and the relatively short wavelengths of light used to activate the PS. While well-oxygenated tumors that are superficial may respond well to traditional PDT, some of the most aggressive and drug-resistant tumors,^{10,11} including solid tumors, have proven to be a challenge that the metal complexes may be able to overcome.

It is generally accepted that the triplet excited states of PSs exert their PDT effects through energy or electron transfer to ground state oxygen to produce reactive oxygen species (ROS), most notably $^1\text{O}_2$. Thus, PSs with appropriate triplet energy levels, high quantum yields for triplet state formation, and long intrinsic triplet lifetimes are highly desirable for PDT. Intersystem crossing (ISC) is fast in metal complexes due to the heavy atom effect, and this is desirable for efficient triplet state formation. However, fast ISC back to the ground state also limits the intrinsic lifetime of the reactive triplet excited state, giving far less time for efficient bimolecular interactions that are critical for photocytotoxic effects. One way to mitigate this issue while maintaining fast ISC rates for triplet state formation is to utilize spin-forbidden transitions in organic chromophores. For example, we have demonstrated that ruthenium (Ru) complexes equipped with ligands either contiguously fused^{12,13} or tethered^{9,14–16} to π -expansive organic chromophores produce very potent *in vitro* PDT effects that are presumably due to very long intrinsic triplet lifetimes. The idea of a metal–organic dyad construct that installs a spatially-separated pendant organic chromophore in a Ru(II) complex for generating long-lived triplets was first put forward by Ford and Rodgers¹⁷ and later expanded by others.¹⁸ Turro and coworkers extended this idea further by showing that contiguously fused π -expansive ligands such as benzo[*l*]dipyrido[3,2-*a*:2',3'-*c'*]phenazine (dppn) also produced long-lived triplets in Ru(II) dyads, and demonstrated that these agents act as potent DNA photocleavage agents.¹⁹ Inspired by these studies, we have focused on developing a variety of transition-metal complexes with π -expansive ligands as PDT agents using both approaches.

While cyclometalated Ir(III) complexes have been extensively studied in organic light-emitting diodes^{20,21} and light-emitting electrochemical cells,^{22,23} PSs^{24,25} and photocatalysts,^{26–28} very few Ir(III) complexes as PSs for *in vitro* PDT have been reported.^{29–32} This is despite Ir(III) having one of the largest

spin-orbit coupling (SOC) constants known (3909 cm^{-1})³³ and consequently very high quantum yields for triplet state formation.^{34,35} We have recently shown that biscyclometalated Ir(III) complexes with long triplet state lifetimes have favorable properties for both reverse saturable absorption (RSA) and PDT.³⁶ These systems were characterized by π -expansive ligands with systematic variations in the two identical cyclometalating ligands as well as the diimine ligand. Light-enhanced cytotoxicities were as low as 3 nM with phototherapeutic indices (PIs) greater than 400 at relatively soft light doses.

In the search for better PSs that combine therapeutic, imaging and targeting capabilities into a single molecule,³⁷ we have continued our exploration of such promising biscyclometalated Ir(III) complexes as PSs for PDT. Ir(III) complexes have the potential to act simultaneously as therapeutic and diagnostic (theranostic) agents owing to their large luminescence quantum yields^{38–40} and excitation/emission energies that can be easily tuned by varying the structure and substituents of the cyclometalating and/or the ancillary diimine ligand, thus covering almost the entire visible spectrum.^{41–43}

Near-infrared (NIR) emitting Ir(III) complexes, however, are relatively rare,^{44–46} but highly desirable for bioimaging and labeling.⁴⁰ The biscyclometalated Ir(III) complexes reported herein were designed as NIR emitters to add diagnostic capacity to their predicted *in vitro* PDT effects. Phosphorescent cyclometalated cationic Ir(III) complexes are good candidates as they possess (1) large Stokes shifts (more than 100 nm) to avoid inner filter effects; (2) rapid transmembrane activity (short incubation time and less potential toxicity); (3) long luminescence lifetimes (100 ns to 1 ms) for time-resolved detection; and (4) enhanced photostabilities (less photobleaching). Photostability is particularly important for allowing continuous exposure of the complexes to irradiation and enabling real-time monitoring of the probes. All of these features are highly desirable for a theranostic PDT agent.

In this report we utilize the π -expansive 2,3-diphenylbenzo[*g*]quinoxaline as the two cyclometalating (C[^]N) ligands and probe the effects of systematic changes to the identity of the diimine ligand (Chart 1) on the photophysical and photobiological properties of the resulting complexes. We also demonstrate their NIR phosphorescence in live cells, underscoring their theranostic potential.

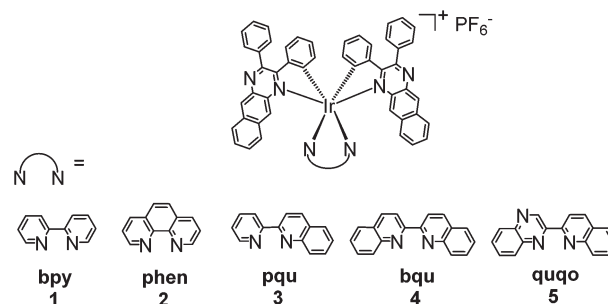


Chart 1 Molecular structures of the cationic iridium complexes 1–5.

Experimental section

Synthesis and characterization

All reagents and solvents were purchased from commercial sources and used as is unless otherwise mentioned. The spectroscopic grade solvents used for photophysical studies were purchased from VWR International and used as received. ^1H NMR spectra were recorded on a Bruker-400 spectrometer in CDCl_3 with tetramethylsilane (TMS) as the internal standard or in d_6 -DMSO. High resolution mass spectrometry (HRMS) analyses were performed on a Waters Synapt G2-Si mass spectrometer with electrospray ionization (ESI). Elemental analyses were conducted by NuMega Resonance Laboratories, Inc. (San Diego, California). The diimine ligands pqu⁴⁷ and quqo⁴⁸ and the cyclometalating dpbq⁴⁹ ligand were prepared according to the reported procedures while the other ligands (bpy, phen, bqu) were commercially available. The iridium dimer $[\text{Ir}(\text{dpbq})_2\text{Cl}]_2$ was prepared following the Nonoyama method.⁵⁰

General procedure for the synthesis of complexes 1–5. An iridium dimer $[\text{Ir}(\text{dpbq})_2\text{Cl}]_2$ (89 mg, 0.05 mmol), its corresponding diimine ligand (0.1 mmol) and AgSO_3CF_3 (25.7 mg, 0.1 mmol) were added into a 50 mL round-bottom flask. Then CH_2Cl_2 and MeOH (v/v = 20/10 mL) were added as the solvent. The mixture was heated to reflux under an argon atmosphere for 22 hours. When the mixture was cooled to room temperature, 80 mg NH_4PF_6 (0.5 mmol) was added and the mixture was stirred for 3 h at room temperature. After the solvent was removed, the residue was purified by column chromatography (silica gel, $\text{CH}_2\text{Cl}_2/\text{MeOH}$ = 40/1 (v/v)) to give the corresponding complexes.

1. Red solid (85 mg, yield: 74%). ^1H NMR (400 MHz, d_6 -DMSO): δ 9.11 (s, 2H), 8.74 (s, 2H), 8.41–8.38 (d, J = 2.8 Hz, 2H), 8.24–8.16 (m, 6H), 8.03–8.01 (m, 6H), 7.78 (s, 6H), 7.59–7.52 (m, 4H), 7.36 (d, J = 8.0 Hz, 2H), 7.20 (d, J = 8.0 Hz, 2H), 6.82 (t, J = 8.0 Hz, 2H), 6.70–6.67 (m, 4H). ESI-HRMS calcd for $[\text{C}_{58}\text{H}_{38}\text{IrN}_6]^+$ ($\text{M} - \text{PF}_6$): 1011.2792, found: 1011.2788. Anal calcd (%) for $\text{C}_{58}\text{H}_{38}\text{IrN}_6\text{PF}_6$: C, 60.25; H, 3.31; N, 7.27. Found: C, 60.27; H, 3.65; N 6.89.

2. Red solid (65 mg, yield: 69%). ^1H NMR (400 MHz, d_6 -DMSO): δ 9.53–9.52 (d, J = 4.0 Hz, 2H), 8.86–8.83 (d, J = 8.0 Hz, 2H), 8.63 (s, 2H), 8.59–8.55 (m, 2H), 8.08–8.05 (m, 6H), 8.02–8.00 (d, J = 8.0 Hz, 4H), 7.80–7.79 (m, 6H), 7.53–7.46 (m, 4H), 7.34–7.32 (d, J = 8.0 Hz, 2H), 7.27–7.25 (d, J = 8.0 Hz, 2H), 6.89–6.85 (m, 2H), 6.74–6.73 (m, 4H). ESI-HRMS calcd for $[\text{C}_{60}\text{H}_{38}\text{IrN}_6]^+$ ($\text{M} - \text{PF}_6$): 1035.2792, found: 1035.2788. Anal calcd (%) for $\text{C}_{60}\text{H}_{38}\text{IrN}_6\text{PF}_6 \cdot \text{H}_2\text{O}$: C, 60.14; H, 3.36; N, 7.01. Found: C, 60.52; H, 3.33; N, 7.10.

3. Red solid (65 mg, yield: 54%). ^1H NMR (400 MHz, d_6 -DMSO): δ 8.89 (s, 1H), 8.82 (s, 1H), 8.77–8.75 (d, J = 8.0 Hz, 1H), 8.66–8.60 (m, 3H), 8.38–8.30 (m, 3H), 8.19–8.17 (d, J = 8.0 Hz, 2H), 8.13–8.10 (t, J = 4.0 Hz, 1H), 8.05–7.95 (m, 4H), 7.78–7.76 (m, 3H), 7.64–7.45 (m, 8H), 7.38 (s, 1H), 7.28–7.26 (d, J = 8.0 Hz, 1H), 7.24–7.20 (t, J = 8.0 Hz, 1H), 7.09–7.07 (d, J = 8.0 Hz, 1H), 6.90–6.85 (t, J = 8.0 Hz, 1H), 6.80–6.76 (m, 2H), 6.71–6.59 (m, 5H), 6.11–6.09 (d, J = 8.0 Hz, 1H). ESI-HRMS calcd for $[\text{C}_{62}\text{H}_{40}\text{IrN}_6]^+$ ($\text{M} - \text{PF}_6$): 1061.2949, found:

1061.2939. Anal calcd (%) for $\text{C}_{62}\text{H}_{40}\text{IrN}_6\text{PF}_6 \cdot \text{H}_2\text{O}$: C, 60.83; H, 3.46; N, 6.86. Found: C, 60.86; H, 3.36; N 6.67.

4. Red solid (65 mg, yield: 52%). ^1H NMR (400 MHz, d_6 -DMSO): δ 8.86 (m, 4H), 8.56–8.53 (d, J = 8.0 Hz, 2H), 8.28–8.26 (d, J = 8.4 Hz, 2H), 8.16–8.14 (d, J = 8.4 Hz, 2H), 7.98 (s, 2H), 7.85–7.81 (t, J = 8.0 Hz, 2H), 7.70–7.48 (m, 12H), 7.38–7.25 (m, 6H), 6.97–6.95 (d, J = 8.4 Hz, 2H), 6.90–6.87 (t, J = 8.0 Hz, 2H), 6.80–6.78 (d, J = 8.0 Hz, 2H), 6.74–6.70 (t, J = 8.0 Hz, 2H), 6.21–6.19 (d, J = 8.0 Hz, 2H). ^{13}C NMR (101 MHz, d_6 -DMSO) δ 165.40, 159.54, 154.11, 152.79, 146.95, 144.05, 142.47, 139.41, 137.25, 136.29, 133.46, 133.33, 132.73, 132.58, 132.36, 132.00, 130.61, 130.50, 130.02, 129.32, 129.09, 128.80, 128.65, 128.21, 127.58, 127.24, 122.60, 122.48, 122.44. ESI-HRMS calcd for $[\text{C}_{66}\text{H}_{42}\text{IrN}_6]^+$ ($\text{M} - \text{PF}_6$): 1111.3105, found: 1111.3098. Anal calcd (%) for $\text{C}_{66}\text{H}_{42}\text{IrN}_6\text{PF}_6 \cdot 1.4\text{H}_2\text{O}$: C, 60.63; H, 3.49; N, 6.39. Found: C, 60.92; H, 3.89; N 6.09.

5. Red solid (50 mg, yield: 40%). ^1H NMR (400 MHz, d_6 -DMSO): δ 9.90 (s, 1H), 8.94–8.75 (m, 4H), 8.40–8.38 (d, J = 8.0 Hz, 1H), 8.31–8.30 (d, J = 8.0 Hz, 1H), 8.19–8.10 (m, 4H), 7.88 (t, J = 6.0 Hz, 1H), 7.72–7.21 (m, 19H), 6.98 (t, J = 6.0 Hz, 1H), 6.78–6.72 (m, 7H), 6.35–6.33 (d, J = 8.0 Hz, 1H), 6.21–6.19 (d, J = 8.0 Hz, 1H). ESI-HRMS calcd for $[\text{C}_{65}\text{H}_{41}\text{IrN}_7]^+$ ($\text{M} - \text{PF}_6$): 1112.3058, found: 1112.3042. Anal calcd (%) for $\text{C}_{65}\text{H}_{41}\text{IrN}_7\text{PF}_6$: C, 62.10; H, 3.29; N, 7.80. Found: C, 61.74; H, 3.35; N 7.54.

Anion exchange to chloride. Amberlite IRA-410 ion exchange resin (30 g, Aldrich catalog # 06433) was soaked in 200 mL of 1 M HCl for 3 days at 50 °C. After this swelling procedure, the resin and acid were poured into a column. The acid was drained and the column was rinsed with CH_3OH five times to ensure the complete removal of acid from the resin. The pure complexes were dissolved in a small amount of CH_3CN and then loaded on the column. Elution with CH_3OH afforded the target complexes as chloride salts.

Photophysical studies

The ultraviolet-visible (UV-vis) absorption spectra were recorded on a Varian Cary 50 spectrophotometer. Steady-state emission spectra were obtained with 473 nm excitation and an InGaAs array (spectral response range: 0.9–1.7 μm) as the detector and a 500 nm long pass filter to block the excitation beam. A NIR dye IR-26 (Φ = 0.0005)⁵¹ was used as the reference for the emission quantum yield measurement. The emission spectra upon excitation at shorter wavelengths were recorded on a Horiba Jobin Yvon FluoroMax-4 fluorometer/phosphorometer that is equipped with a Hamamatsu photomultiplier tube (PMT) R928 (spectral response range: 185–900 nm) as the detector. The nanosecond transient difference absorption (TA) spectra and decay characteristics were measured in degassed CH_3CN solutions on an Edinburgh LP-920 laser flash photolysis spectrometer. The third harmonic output (355 nm) of a Nd:YAG laser (Quantel Brilliant, pulse width = 4.1 ns, repetition rate = 1 Hz) was used as the excitation source. Each sample solution was purged with argon for 45 min prior to measurement.

Singlet oxygen quantum yields

Singlet oxygen emission from dilute solutions (5 μM) of the PF_6^- salts of the complexes in spectroscopic-grade CH_3CN was measured using a PTI Quantamaster equipped with a Hamamatsu R5509-42 near-infrared PMT. Quantum yields for singlet oxygen emission (Φ_Δ) were calculated relative to $[\text{Ru}(\text{bpy})_3](\text{PF}_6)_2$ as the standard ($\Phi_\Delta = 0.56$ in aerated CH_3CN ⁵²) according to eqn (1), where I , A , and η are integrated emission intensity, absorbance at the excitation wavelength, and refractive index of the solvent, respectively. The calculated Φ_Δ was reproducible to within <5%.

$$\Phi_\Delta = \Phi_{\Delta s} \left(\frac{I}{I_s} \right) \left(\frac{A_s}{A} \right) \left(\frac{\eta^2}{\eta_s^2} \right) \quad (1)$$

Computational methods

Singlet geometry optimizations of all iridium complexes were performed with density functional theory (DFT) formalism implemented in Gaussian09 software package.⁵³ The time-dependent DFT (TDDFT) method was employed to calculate the absorption spectra of complexes using a Gaussian09 software package as well. The linear response density was calculated within a TDDFT framework,⁵⁴ from which the excitation energies and oscillator strength can be extracted by iteratively solving the eigenvalue equation problem based on Davidson algorithm.^{55–58} Forty optical transitions were calculated to obtain the absorption spectra at an energy range comparable to the experimental UV-vis spectra.

To obtain the fluorescence emission energies, we optimized the lowest singlet excited state geometry using the TDDFT analytical approach.⁵⁹ To obtain the phosphorescence emission energies, we first optimized at the lowest triplet ground state geometry using the unrestricted DFT method (ΔSCF approach) within Gaussian09 software. The lowest triplet excitation energy was calculated through the combined scalar relativistic ZORA and TDDFT approach using the NWChem software package. The one-electron energies and orbitals were obtained by solving the one-electron ZORA Kohan–Sham equation.⁵³

The hybrid PBE1 functional⁶⁰ was used for both the ground and excited state calculations. The LANL2DZ basis set was applied for Ir, while the 6-31G* basis set was applied for the remaining atoms. Both geometry optimization and optical absorption calculations were performed in a solvent medium using a conductor-like polarizable continuum model (CPCM),^{61,62} as implemented in Gaussian09. Fluorescence and phosphorescence calculations were performed *via* COSMO continuum solvation^{63,64} as implemented in NWChem. Dichloromethane (CH_2Cl_2 , $\epsilon_r = 9.08$) was chosen as the solvent medium for consistency with experimental studies.

To visualize the excited states that can be represented as hole–electron pairs created upon photoexcitation, natural transition orbitals (NTOs) were provided.^{62,65} By performing NTO calculations implemented in Gaussian09, an electron–hole pair transition from a ground state to an excited state could be realized through unitary transformation of the transition density matrix of a given excited state.⁶² For visualization of the lowest singlet and triplet emitting states, the dominant molecular orbitals contributing to the excited state were plotted by performing the eigenvector analysis of this state. Chemcraft-1.7 software⁶⁶ was used for plotting excited state charge densities by setting the isovalue as 0.02.

Photobiological activity studies

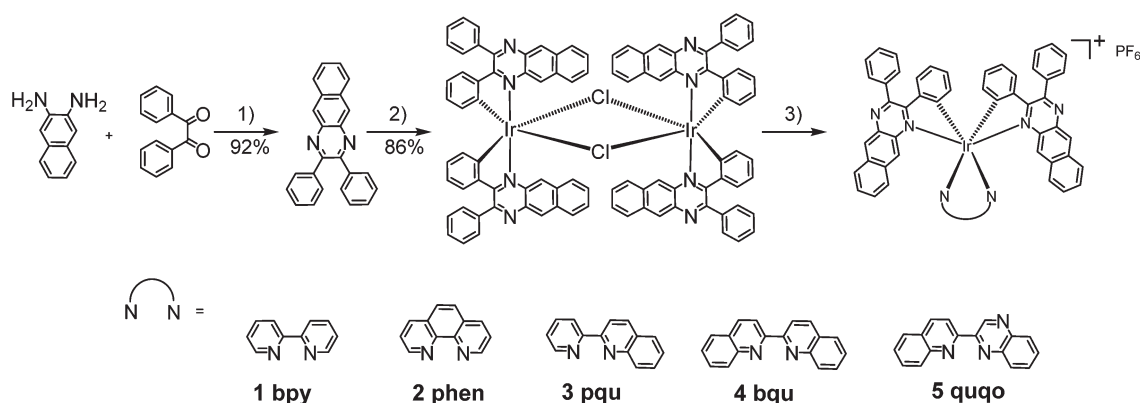
The details of the cell culture, cytotoxicity and photocytotoxicity studies, confocal microscopy, and DNA mobility-shift assays are provided in the ESI.†

Results and discussion

Molecular design and synthesis

Previous studies revealed that the degree of π -conjugation of the $\text{C}^{\wedge}\text{N}$ ligands impacts the emission from Ir(III) complexes dramatically.^{67–69} Introduction of a highly conjugated $\text{C}^{\wedge}\text{N}$ ligand is required to achieve the NIR emission of the complexes.⁴⁴

As shown in Scheme 1, the dpbq ligand was synthesized by a condensation reaction between commercially available



Scheme 1 Synthetic route for complexes 1–5. Reaction conditions: (1) p -TsOH, EtOH, reflux; (2) $\text{IrCl}_3 \cdot 3\text{H}_2\text{O}$, 2-ethoxyethanol/ H_2O , reflux; (3) bpy, AgSO_3CF_3 , $\text{CH}_2\text{Cl}_2/\text{MeOH}$, reflux; then NH_4PF_6 , r.t.

2,3-naphthalenediamine and benzil in absolute ethanol with *p*-TsOH as a dehydration agent in 92% yield. Subsequent reaction of dpbq with $\text{IrCl}_3 \cdot 3\text{H}_2\text{O}$ in a refluxed ethoxyethanol/water ($v/v = 3/1$) mixture resulted in a red precipitate, which was washed with water to give the $[\text{Ir}(\text{dpbq})_2\text{Cl}]_2$ dimer with satisfactory purity. Complexes 1–5 were synthesized by reaction of the $[\text{Ir}(\text{dpbq})_2\text{Cl}]_2$ dimer with the corresponding diimine ligand in mixed CH_2Cl_2 /methanol ($v/v = 1:1$). All the complexes are readily dissolved in CH_2Cl_2 , CH_3CN , and DMSO, but they have limited solubility in nonpolar solvents such as hexane and toluene. All our complexes were purified by column chromatography on silica gel and characterized by ^1H NMR, ESI-HRMS (ESI Fig. S1–S5[†]) and elemental analysis. All

complexes were very stable even in coordinating solvents such as DMSO, as reflected by the absence of detectable decomposition by TLC from the d_6 -DMSO sample solutions kept under ambient conditions in the NMR tubes.

For all of the photophysical studies discussed in the following sections, the PF_6 salts of the complexes were used. The Cl salts of the complexes were used for the photobiological studies.

Electronic absorption

The UV-vis absorption spectra of complexes 1–5 were collected in CH_2Cl_2 , and the results are shown in Fig. 1 and Table 1. Variable concentration experiments confirmed that no ground state aggregation occurred in the concentration range studied (5×10^{-6} to $1 \times 10^{-4} \text{ M}^{-1}$).

The absorption spectra of all complexes featured intense bands at wavelengths below 350 nm with molar extinction coefficients of $6.0\text{--}6.8 \times 10^4 \text{ M}^{-1} \text{ cm}^{-1}$. Based on these large molar extinction coefficients and the natural transition orbitals (NTOs, see ESI Table S1[†]) obtained from the TDDFT calculations, these bands are assigned to the dpbq ligand-localized $^1\pi, \pi^*/^1\text{ILCT}$ transitions with some contributions from the $^1\text{LLCT}/^1\text{MLCT}/^1\text{LMCT}$ transitions. For complex 5, the $^1\pi, \pi^*$ transition from the diimine ligand quqo also made a significant contribution. The absorption bands at 400–500 nm are mainly dpbq ligand-centred $^1\pi, \pi^*/^1\text{MLCT}/^1\text{ILCT}/^1\text{LMCT}$ transitions for all complexes, while complexes 3–5 have $^1\text{LLCT}$ transitions contributing to the 400–470 nm band. For complexes 4 and 5, the diimine ligand-based $^1\pi, \pi^*$ transition also contributed to the 400–470 nm band (see ESI Table S2[†]). All complexes possess a low-energy absorption band between 500 and 600 nm, which mainly arises from the dpbq ligand-associated $^1\text{ILCT}/^1\text{MLCT}$ transitions combined with some $^1\pi, \pi^*$ character (see NTOs in Table 2). For complexes 3–5, contributions from the $^1\text{LLCT}$ transition systematically increased, with the lowest singlet transition (S_1 state) in 5 being switched to the $^1\text{LLCT}/^1\text{MLCT}$ transition. In addition to the aforementioned absorption bands, all complexes displayed very

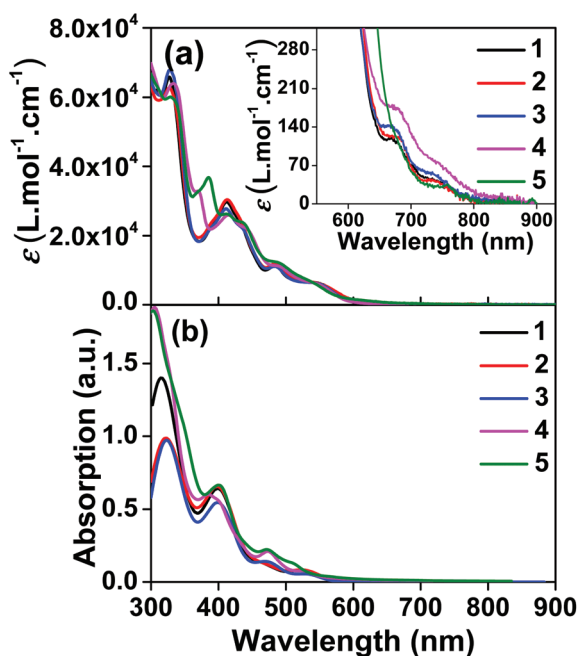


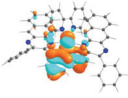
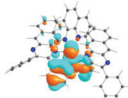
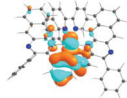
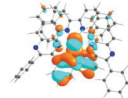
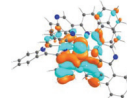
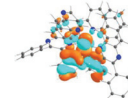
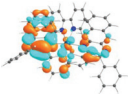
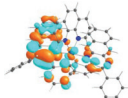
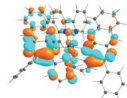
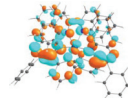
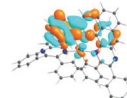
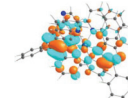
Fig. 1 (a) Experimental and (b) calculated absorption spectra of complexes 1–5 in dichloromethane. The inset in panel (a) shows the expansion of the absorption above 550 nm.

Table 1 Photophysical data for complexes 1–5

| | $\lambda_{\text{abs}}/\text{nm}$ ($\epsilon/10^4 \text{ M}^{-1} \text{ cm}^{-1}$) ^a | $\lambda_{\text{em}}/\text{nm}$; Φ_{em} ^b | τ_0 ^c /ns | $\lambda_{\text{T1-Tn}}/\text{nm}$ ($\tau_{\text{TA}}/\text{ns}$) ^d | Φ_{Δ} ^e |
|---|--|---|---------------------------|--|------------------------------|
| 1 | 327 (6.6), 412 (2.9), 486 (1.1), 550 (0.6), 673 (0.012), 742 (0.004, br) | 794, 911, 965; 0.003 | 440 | 364 (–), 454 (290), 519 (320), 659 (320) | 0.55 (0.42) |
| 2 | 328 (6.3), 413 (3.0), 485 (1.2), 550 (0.7), 681 (0.012), 742 (0.004, br) | 801, 913, 965; 0.0032 | 430 | 374, 450 (350), 522 (350), 668 (350) | 0.47 (0.40) |
| 3 | 328 (6.8), 411 (2.8), 486 (1.1), 546 (0.7), 673 (0.014), 738 (0.005, br) | 794, 910, 964; 0.0025 | 460 | 366, 457 (380), 517 (380), 660 (380) | 0.54 (0.41) |
| 4 | 333 (6.4), 370 (3.3), 416 (2.5), 443 (2.2), 493 (1.1), 545 (0.6), 679 (0.017), 747 (0.007, br) | 801, 916, 968; 0.002 | 370 | 375 (340), 519 (360), 660 (350) | 0.38 (0.33) |
| 5 | 331 (6.0), 385 (3.7), 413 (2.6), 437 (2.4), 490 (1.2), 540 (0.6), 756 (0.003, br) | 800, 915, 970; 0.0017 | 360 | 443 (450 (6%), 4940 (94%)), 508 (420 (14%)), 4820 (86%), 650 (430 (11%), 4960 (89%)) | 0.56 (0.42) |

^a Absorption band maxima and molar extinction coefficients in CH_2Cl_2 at room temperature. ^b Room temperature emission band maxima and emission quantum yields measured in CH_2Cl_2 with an InGaAs sensor upon 473 nm excitation. IR-26 was used as the reference for the NIR emission quantum yield measurements. ^c Intrinsic lifetime in CH_2Cl_2 measured with an Hamamatsu R928 PMT. ^d Triplet transient absorption band maxima and lifetimes in CH_3CN . ^e Singlet oxygen quantum yields at $\lambda_{\text{ex}} = 550 \text{ nm}$, the values in parenthesis are obtained at $\lambda_{\text{ex}} = 412 \text{ nm}$ for 1, 413 nm for 2 and 3, and 417 nm for 4 and 5 in CH_3CN .

Table 2 Natural transition orbitals (NTOs) representing the lowest energy transitions

| | 1 | 2 | 3 | 4 | 5 | |
|------|---|---|---|--|---|---|
| | S ₁ | S ₁ | S ₁ | S ₁ | S ₁ | S ₃ |
| | 531 nm | 531 nm | 533 nm | 528 nm | 565 nm | 512 nm |
| | <i>f</i> = 0.06 | <i>f</i> = 0.05 | <i>f</i> = 0.04 | <i>f</i> = 0.03 | <i>f</i> = 0.005 | <i>f</i> = 0.04 |
| HOTO |  |  |  |  |  |  |
| LUTO |  |  |  |  |  |  |

weak but clearly observable absorption bands between 600 and 800 nm ($\epsilon < 200 \text{ M}^{-1} \text{ cm}^{-1}$). Due to the very small molar extinction coefficients, we attribute these bands to spin-forbidden transitions to the triplet excited states. A similar phenomenon has been reported in other Ir(III) complexes.^{36,67,68,70,71} Compared with the many other reported Ir(III) complexes that contain fewer π -conjugated C^N ligands, the spin-forbidden transitions in complexes 1–5 are much more red-shifted due to the more π -expansive dpbq ligand. It is apparent that the dpbq ligands played a dominant role in contributing to most of the absorption, while the increased π -conjugation of the diimine ligands gradually increased the diimine ligand related ¹LLCT/¹MLCT character in the S₁ state of complexes 3–5. Additionally, the absorption band at 370 nm and 385 nm in 4 and 5, respectively, should have significant contributions from the diimine ligand centred ¹ π, π^* transition.

Photoluminescence

The room-temperature emission from 1–5 were studied in CH₂Cl₂ upon excitation at different wavelengths. The spectra are shown in Fig. 2 and ESI Fig. S8,† and the emission data upon excitation at 473 nm are compiled in Table 1. 473 nm light was used as the excitation wavelength because it is the

only available blue laser source for our instrument equipped with an InGaAs array detector, and it was capable of exciting both the samples and the IR-26 NIR reference dye with sufficiently bright signals. Upon 473 nm excitation, the emission spectra of all complexes resembled each other and were similar to that of the [Ir(dp bq)₂Cl]₂ dimer (ESI Fig. S9†). The deoxygenated emission lifetimes were between 360 and 460 ns. These observations point toward a common triplet excited state for all of the complexes, which is localized on the same ligand type, *i.e.* the C^N ligand. NTOs from the TDDFT calculations (ESI Table S3†) confirmed that both the electrons and holes are predominantly localized on the C^N ligands. Therefore, the emitting triplet excited states have been ascribed to the C^N ligand centred ³ π, π^* state mixed with some ³LLCT/³MLCT/³LLCT character. The quantum yields for all complexes were very low (near 10^{−3}), which is in agreement with those reported by other groups for similar complexes that contain dpbq as the C^N ligand.⁴⁹ Small quantum yields are not surprising given that the decreased energy of the emitting state (into the NIR) facilitates radiationless decay to the ground state (energy gap law).^{72,73} Although the low emission quantum yields of complexes 1–5 may limit their utility in organic light emitting diodes (OLEDs), their luminescence is strong enough for NIR bioimaging applications,⁷⁴ which will be discussed and demonstrated in the following section.

In contrast, upon excitation at 330 or 370 nm and monitoring with the Hamamatsu PMT R928, complexes 1–4 exhibited dual emission (ESI Fig. S8†). In addition to the NIR emission discussed in the previous paragraph, a broad featureless red emission was observed around 600 nm. This phenomenon resembles that observed from complex 6 in ref. 36 that contains the same dpbq C^N ligand. Considering the structureless feature and the emission energy, we assign this red emission band to the ³MLCT/³LLCT emitting state. Such an attribution is consistent with the ³MLCT/³LLCT emission reported in other Ir(III) complexes with the same or similar diimine ligand.^{36,69,71} The different natures of the red and NIR emission bands are supported by the difference in their excitation spectra monitored at the band maxima of these two emission bands (ESI Fig. S10†). The observation of the dual emission in

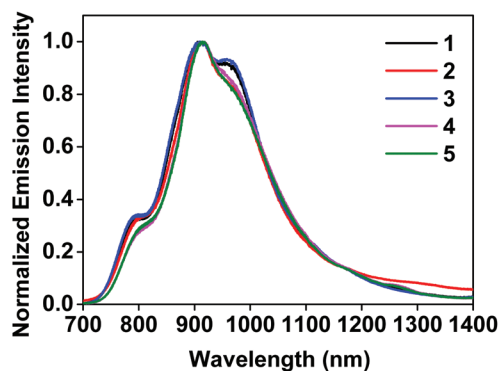


Fig. 2 Normalized emission spectra of complexes 1–5 in deoxygenated CH₂Cl₂ at room temperature using an InGaAs array as the detector and $\lambda_{\text{ex}} = 473 \text{ nm}$.

complexes 1–4 but not in 5 could be attributed to the larger energy difference between the high-lying $^3\text{MLCT}/^3\text{LLCT}$ state and the lowest-energy dpbq ligand centred $^3\pi,\pi^*$ state (T_1 state) in 1–4.⁷¹ With further extended π -conjugation and the stronger electron-withdrawing ability of the quinoxaline group in the diimine ligand of 5, the $^3\text{MLCT}/^3\text{LLCT}$ state in 5 is further stabilized and energetically closer to the dpbq ligand centred $^3\pi,\pi^*$ state.⁷⁰ In such a case, dual emission could not be observed. Although dual emission is unusual, it has been reported in other transition-metal complexes including Ir(III) and Ru(II) complexes.^{14,36,75–84}

It is worth pointing out that the feature of the NIR emission bands shown in ESI Fig. S8† for complexes 1–4 appeared to be different from those in Fig. 2. The difference arose from the different spectral responses and sensitivities of the detectors used in these two measurements. The spectra shown in Fig. 2 were measured with an InGaAs array (spectral response range: 0.9–1.7 μm) that is sensitive to the NIR emission and allows the full NIR spectra of these complexes to be recorded. In contrast, the spectral response range of the Hamamatsu PMT R928 is 185–900 nm, which allows both the red emission and part of the NIR emission to be collected but the detector sensitivity dramatically decreases beyond 800 nm and the emission beyond 850 nm cannot be observed.

Transient absorption (TA)

The triplet excited-states of complexes 1–5 were further investigated by nanosecond transient absorption (TA) spectroscopy. The TA spectra of 1–5 at zero-time-delay recorded upon excitation at 355 nm at room temperature in deaerated acetonitrile solution are shown in Fig. 3, and the time-resolved nanosecond TA spectra of 1–5 are shown in Fig. S11†.

The TA spectra of all complexes were characterized by positive signals at 360–800 nm. The shapes of the TA spectra and the associated decay lifetimes of 1–4 all resemble those of the $[\text{Ir}(\text{dpbq})_2\text{Cl}]_2$ dimer,⁶⁸ indicating that the absorbing triplets were most likely $^3\pi,\pi^*/^3\text{CT}$ states centered on the coordinated dpbq ligand. The agreement between the TA and emission life-

times implies the same orbital parentage of the TA and emitting states, *i.e.* the coordinated dpbq ligand centred $^3\pi,\pi^*$ state combined with an $^3\text{ILCT}/^3\text{MLCT}/^3\text{LLCT}$ character as discussed in the photoluminescence section. However, on going from complex 1 to 4, the ΔOD values decreased with increasing π -conjugation of the diimine ligand. In fact, the bands near 450 nm gradually decreased and eventually became indistinguishable from the 510 nm band in complex 4. This is likely related to the increased ground-state absorption in this spectral region in 4. The TA spectral features of 5 resembled those of 1–4 in the region of 480–800 nm. However, an intense absorption band appeared near 440 nm, which was distinct from the spectra of 1–4. The shape and energy of this band matched well with the TA band of the quqo ligand (ESI Fig. S12†). In addition, the decay profiles at the TA band maxima of 5 were bi-exponential, with a longer lifetime of approximately 5 μs and a shorter lifetime of 420 ns (see Table 1). The longer lifetime is in agreement with the TA lifetime of the quqo ligand (5.87 μs at 440 nm) while the shorter lifetime is similar to the coordinated dpbq ligand-centred $^3\pi,\pi^*/^3\text{CT}$ excited state. Therefore, it appears that the observed TA spectrum of 5 has TA features of both the quqo ligand and the $[\text{Ir}(\text{dpbq})_2\text{Cl}]_2$ dimer. The possibility of the longer-lived species being from a trace amount of non-coordinated quqo ligand was excluded based on the absence of the quqo fluorescence at 480 nm.

Singlet oxygen generation

The complexes were analyzed for their ability to generate $^1\text{O}_2$ by direct measurement of $^1\text{O}_2$ emission centred at 1270 nm. $[\text{Ru}(\text{bpy})_3](\text{PF}_6)_2$, with a reported singlet oxygen quantum yield (Φ_Δ) of 0.56 in aerated CH_3CN ⁵² was used as the standard. Despite the most intense absorption and excitation maxima appearing at wavelengths shorter than 500 nm, the largest $^1\text{O}_2$ quantum yields were produced with excitation at 550 nm for all of the complexes. The calculated values of Φ_Δ for the complexes ranged from 38 to 56% ($\pm 5\%$) (Table 1). Complexes 1, 3, and 5 generated $^1\text{O}_2$ with about the same efficiency as the standard (54–56%). Complexes 2 and 4 were less efficient, with $\Phi_\Delta = 47\%$ and 38%, respectively. These $^1\text{O}_2$ quantum yields were dependent on the nature of the initially populated excited states, and were attenuated with shorter wavelength excitation. For example, Φ_Δ for all of the complexes except 4 was reduced to 40–42% (Table 1) with excitation between 412 and 417 nm, where the absorption and excitation maxima were most intense. Complex 4 also underwent a reduction in Φ_Δ to 33% with 417 nm excitation. Although not exceptionally high, this $^1\text{O}_2$ production was anticipated to result in some photocytotoxicity in cellular assays.

Cytotoxicity and photocytotoxicity assays

The photobiological activities of the five Ir(III) complexes were assessed in the SK-MEL-28 melanoma cell line. The effective concentration required to reduce cell viability to 50% (EC_{50}) was determined from sigmoidal fits of the dose-response curves between 1 nM and 300 μM PS with (light EC_{50}) or

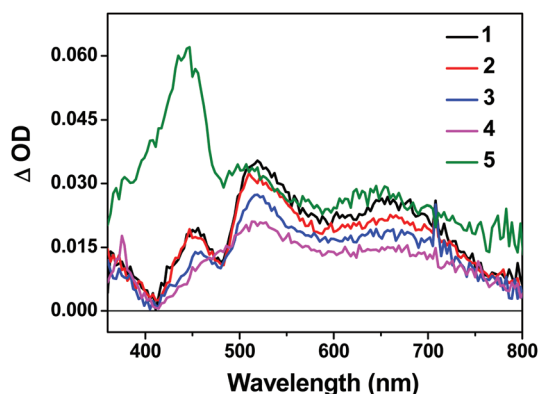


Fig. 3 Nanosecond TA spectra of complexes 1–5 in acetonitrile solution ($\lambda_{\text{ex}} = 355$ nm, $A_{355} = 0.4$ in a 1 cm cuvette) immediately after excitation.

without (dark EC_{50}) a light treatment. The light treatment was broadband visible or single-wavelength red (625 nm) light delivered at a fluence of 100 J cm^{-2} and irradiance of 35.7 mW cm^{-2} and 32.3 mW cm^{-2} for visible and red, respectively. The phototherapeutic index (PI) was calculated as the ratio of dark to light EC_{50} values and is a measure of the therapeutic margin for *in vitro* PDT. Additionally, the dark cytotoxicity was measured in normal skin fibroblasts (CCD-1064Sk) to determine any selectivity for cancer cells over normal cells. The selectivity factor (SF) is defined as the ratio of the dark EC_{50} value measured for CCD-1064Sk cells and the dark EC_{50} value measured for SK-MEL-28 cells. As long as the dark cytotoxicity toward normal cells is low and the PI large, $SF > 1$ is not a requirement. PDT is inherently selective with spatial and temporal control of light delivery.

The dark cytotoxicities toward melanoma cells for the Ir(III) complexes varied from 230 nM to $18 \mu\text{M}$, and increased in the order: $3 > 2 > 4 > 5 > 1$ (Table 3, Fig. 4 and ESI Fig. S13†). When compared with noncancerous skin fibroblasts, complexes 2 and 3 were up to 40-fold more cytotoxic toward the melanoma cells while 1, 4, and 5 displayed almost no selectivity for the cancer cells (ESI Table S4†). The relatively simple change in the identity of the diimine ligand from bpy in complex 1 to phen in complex 2 increased the dark cytotoxicity toward melanoma cells by more than 50-fold. Benzannulation at C5–C6 to form pqu produced an Ir(III) complex 3 that was almost 80-times more dark cytotoxic relative to 1. However, a second benzannulation to form the symmetric bqu as in complex 4 increased dark cytotoxicity toward the cancer cells by only 6-fold relative to 1. Replacement of one of the quinoline rings with quinoxaline in complex 5 did not substantially alter the dark toxicity. Increased π -expansion on the diimine ligand in complexes 2 and 3 does appear to increase dark cytotoxicity toward the melanoma cells relative to bpy. However, the dark cytotoxicity toward melanoma cells does not directly correlate with the lipophilicity index of the diimine ligand in this class of complexes. Interestingly, the dark cytotoxicity toward normal skin fibroblasts increased in the order $4 > 5 > 3 > 2 > 1$, which did more closely parallel the lipophilicity index of the diimine ligand. The substantial deviation in the trend observed for complexes 2 and 3 in melanoma cells

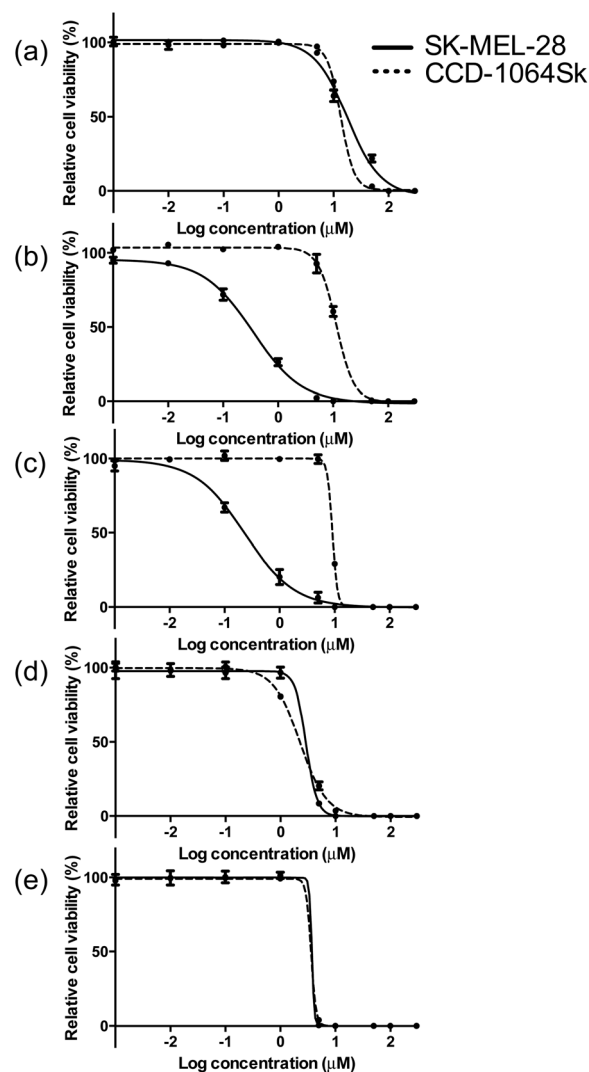


Fig. 4 Comparison of dark cytotoxicity for complexes 1 (a), 2 (b), 3 (c), 4 (d) and 5 (e) in SK-MEL-28 (solid line) and CCD-1064Sk cells (dotted line).

Table 3 Photobiological activities for SK-MEL-28 cells dosed with complexes 1–5

| Complex ^a | Dark | | Visible | | Red | |
|----------------------|-----------------------------|-----------------|-----------------------------|-----------------|-----------------------------|-----------------|
| | EC_{50} (μM) | SF ^b | EC_{50} (μM) | PI ^c | EC_{50} (μM) | PI ^c |
| 1 | 17.9 ± 2.27 | 0.8 | 0.25 ± 0.02 | 71 | 1.71 ± 0.12 | 10 |
| 2 | 0.34 ± 0.03 | 34 | 0.015 ± 0.001 | 23 | 0.16 ± 0.05 | 2.1 |
| 3 | 0.23 ± 0.03 | 40 | 0.018 ± 0.004 | 13 | 0.15 ± 0.01 | 1.5 |
| 4 | 2.92 ± 0.68 | 0.8 | 0.12 ± 0.01 | 24 | 2.11 ± 0.21 | 1.4 |
| 5 | 3.27 ± 0.14 | 1.1 | 0.012 ± 0.001 | 273 | 0.20 ± 0.01 | 16 |

^a Complexes screened as their chloride salts. ^b SF = selectivity factor.

^c PI = phototherapeutic index.

resulted in very large SFs, making these complexes of interest as traditional chemotherapeutics.

The visible light EC_{50} values measured in melanoma cells ranged from 12 to 252 nM, with complex 5 being the most photocytotoxic (Table 3, Fig. 5 and ESI Fig. S13†). As expected, *in vitro* red light PDT was attenuated 10- to 20-fold relative to the more energetically visible light treatment, with red light EC_{50} values spanning 150 nM to $2.1 \mu\text{M}$. Photocytotoxicity increased in the order $5 \approx 2 \approx 3 > 4 > 1$ for visible PDT and $3 \approx 2 \approx 5 > 1 > 4$ for red PDT. Generally speaking, complexes 2, 3, and 5 clustered around 15 nM for visible PDT and 170 nM for red PDT, while 1 and 4 clustered around 190 nM for visible PDT and $1.9 \mu\text{M}$ for red PDT. These results demonstrate that phen, pqu, and quqo as coligands were the most effective at increasing photocytotoxic effects, while bpy and bqu were less effective. Similar to the dark toxicity trends, benzannulation had the effect of increasing phototoxicity. However, replace-

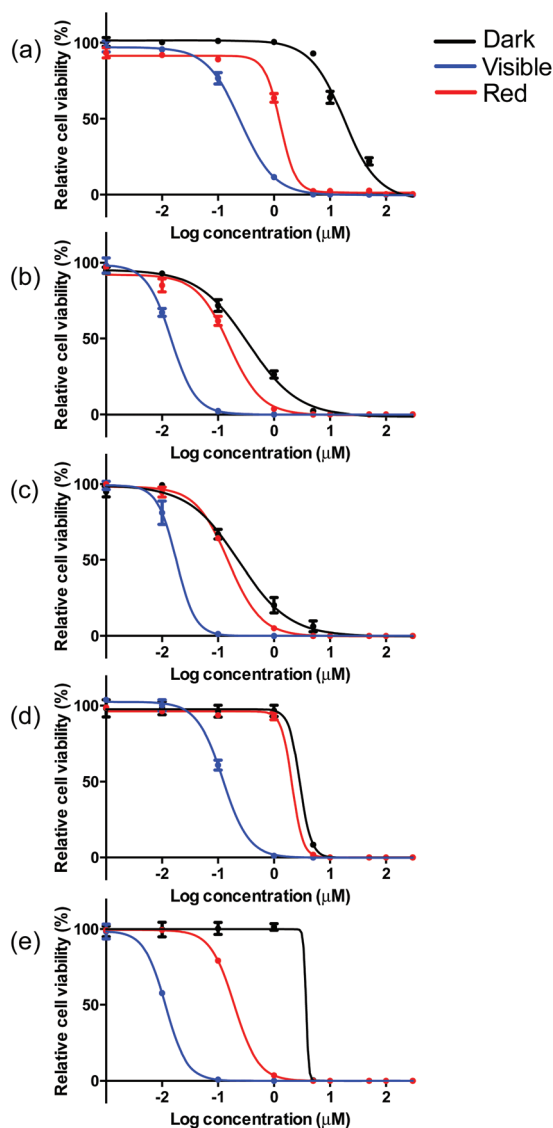


Fig. 5 *In vitro* dose-response curves for complexes 1 (a), 2 (b), 3 (c), 4 (d) and 5 (e) in SK-MEL-28 cells treated in the dark (black) and with visible (blue) or red (red) light activation.

ment of C4 with N on going from 4 to 5 increased photocytotoxicity, whereas this change had only a marginal effect on dark toxicity (with 5 being slightly less dark toxic).

These photocytotoxicity trends could not be directly correlated to differences in absorption coefficients, emission quantum yields, or TA/emission lifetimes. When considering complexes 2–5, larger photocytotoxicities generally paralleled $^1\text{O}_2$ quantum yields, whereby complex 4 with the smallest value for Φ_{Δ} , was approximately ten-fold less phototoxic. However, complex 1 was the least phototoxic of the series despite being among the more efficient singlet $^1\text{O}_2$ sensitizers. While cell-free $^1\text{O}_2$ experiments do not directly correlate with *in vitro* cellular conditions, it appears that factors other than singlet oxygen generation may govern the *in vitro* PDT effects of this class of Ir(III) complexes.

Taken together, the dark and light cytotoxicities yielded respectable PDT effects for certain members of this class of complexes (Table 3, Fig. 5 and S13†). Complex 5 produced the largest PDT effects in this series, with a PI > 270 for visible light and >15 for red light. Complex 1 was also an effective PDT agent (visible PI > 70, red PI = 10), but was almost four-fold less effective than 5. Complexes 2–4 were the least effective PDT agents, and yielded PIs between 10 and 25 for visible light and up to only 2 for red light. Given that the light EC_{50} values for 2, 3, and 5 did not differ substantially between the two light treatments, yet 5 had a 20-fold larger phototherapeutic margin, the underlying factor governing the PDT effects in this class of complexes appears to be dark toxicity.

Cellular imaging

Phosphorescence from this class of Ir(III) complexes proved to be a convenient tool for monitoring uptake by SK-MEL-28 melanoma cells with and without a light treatment (Fig. 6). Excitation for confocal imaging was performed by using an argon-krypton laser (458/488 nm) and emission was collected through a 475 nm long pass filter. The images were captured after subjecting the complexes to a brief cellular incubation time (1 h) to ensure sub-lethal conditions. All of the complexes were taken up by cells even in the absence of a light trigger, indicating that the large differences in dark toxicity may not be due to differences in cellular uptake if it is assumed that the intensity of intracellular luminescence is proportional to concentration. This uptake was enhanced with illumination as would be expected with PDT inflicted damage to the cellular membranes. The differences in dark toxicity for the complexes could be easily discerned by changes in cellular morphology. For example, complex 1 was the least toxic in the absence of a light trigger, while complexes 2 and 3 were the most toxic. Cells treated with complex 1 (Fig. 6, diffuse interference contrast (DIC) image) retained their dendritic morphology while only dead/dying cells and debris could be discerned for samples exposed to complex 2. Fig. 6 captured the change in morphology from dendritic to detached spherical, an intermediate stage between viable and dead, quite well for complex 5. It should be noted that the incubation time and light treatment for the confocal imaging was different from that used for the *in vitro* assays to ensure that some cells would be viable for imaging in each sample. Because the *in vitro* cell assay conditions and the confocal imaging conditions were different, a quantitative assessment of overall cytotoxicity and photocytotoxicity by visualization of morphological changes was not attempted. Rather the purpose of the cellular imaging experiment was to highlight that the inherent phosphorescence from the complexes can be used for imaging cellular uptake and localization, and that the morphological changes that accompany cell death do parallel the results from the quantitative *in vitro* measurements regarding toxicity.

DNA interactions

In order to determine whether light-mediated DNA damage could be a factor in the *in vitro* PDT effects observed for this

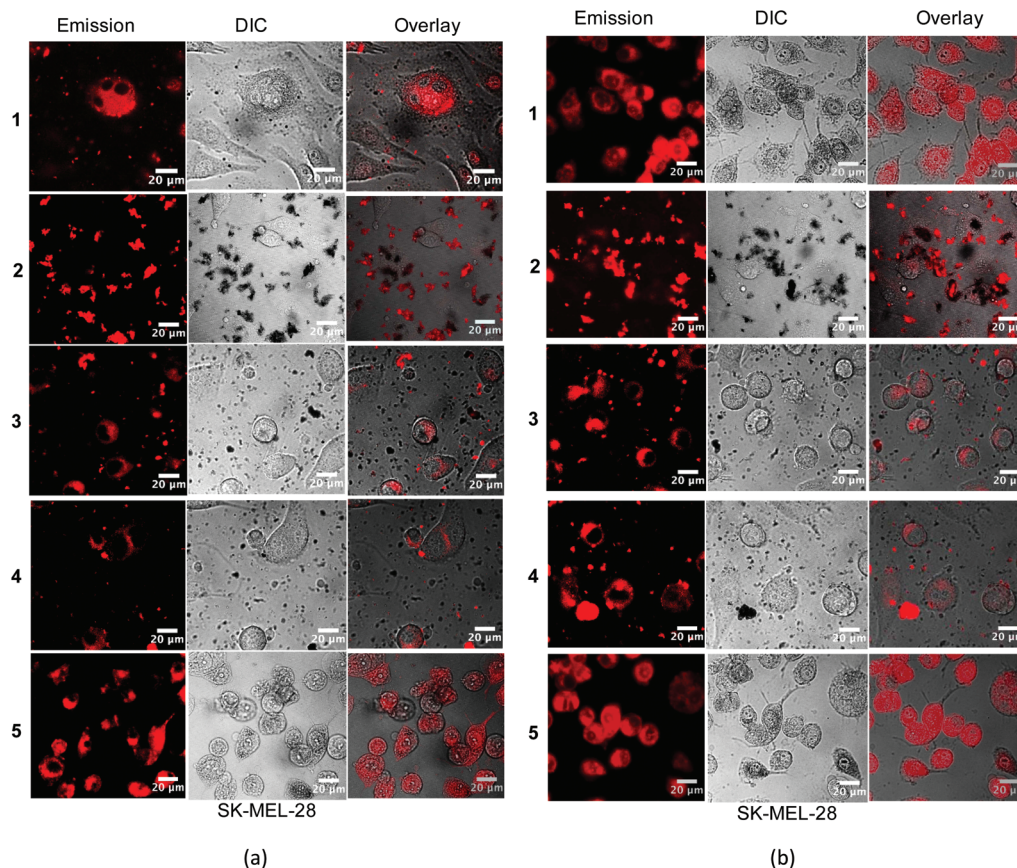


Fig. 6 Confocal luminescence images of SK-MEL-28 cells dosed with complexes 1–5 (50 μM) (a) in the dark and (b) with visible light (50 J cm^{-2}) activation.

class of complexes, supercoiled plasmid DNA (20 μM bases) was exposed to increasing concentrations of 1–5 and light treatment (Fig. 7, lanes 3–8) and compared with DNA alone (lanes 1 and 2) or DNA treated with complexes but no light (lane 9). In this gel electrophoretic mobility shift assay,^{16,84,85} undamaged supercoiled DNA (Form I) migrates the farthest through the gel, while aggregated DNA or condensed DNA (Form IV) hardly moves under the electrophoretic conditions employed. If single strand breaks occur to form relaxed circular DNA (Form II), the DNA migrates farther than form IV but slower than Form I. Frank double strand breaks or single strand breaks on opposing strands (within about 16 base pairs) produce linear DNA (Form III). When plasmid DNA was exposed to 1–5 and light, detectable amounts of Form IV DNA were observed at [MC]:[bases] ratios as low as 1 (lane 4). Increases in Form II (or Form III) DNA were not observed and indicated that the most prominent interaction with DNA is the induction of aggregation rather than strand breaks.

Disappearance of gel bands at higher complex concentrations with or without light treatment precluded a quantitative comparison of the relative strengths of the complex–DNA interactions, although qualitatively the interactions appeared very similar. A lack of DNA staining could be attributed to quenching of the fluorescence from DNA stain ethidium

bromide (EtBr), competition for EtBr intercalation sites, or distortion of the helix (that prevents EtBr binding) caused by complex binding. Interestingly, complex 1 did not cause disappearance of bands even at high concentration but did induce a similar aggregation pattern as observed for the other complexes before the bands became too faint to analyze. The conversion from Form I to Form IV DNA by 1 occurred with no accompanying DNA photocleavage, indicating that DNA damage by singlet oxygen did not occur (normally observed as strand breaks to yield detectable Form II⁸⁶). The absence of photoinduced Form II DNA was also evident for 1–4 as direct conversion of Form I to Form IV before the signal from Form IV disappeared. Given the similarities in the DNA aggregation profiles produced by 1–5 and the variation in their dark and light cytotoxicities, it might be inferred that DNA is not an important intracellular target. Moreover, the absence of Form II DNA points toward a mechanism for photocytotoxicity that does not involve singlet oxygen. However, the cell-free experiments do not mimic the complexity of the cellular environment and dynamic processes, which involve uptake, efflux, metabolism, and localization. Thus *in vitro* DNA targeting and singlet oxygen damage cannot be discounted with certainty. Efforts are underway to understand the cellular targets and the underlying mechanism for *in vitro* PDT.

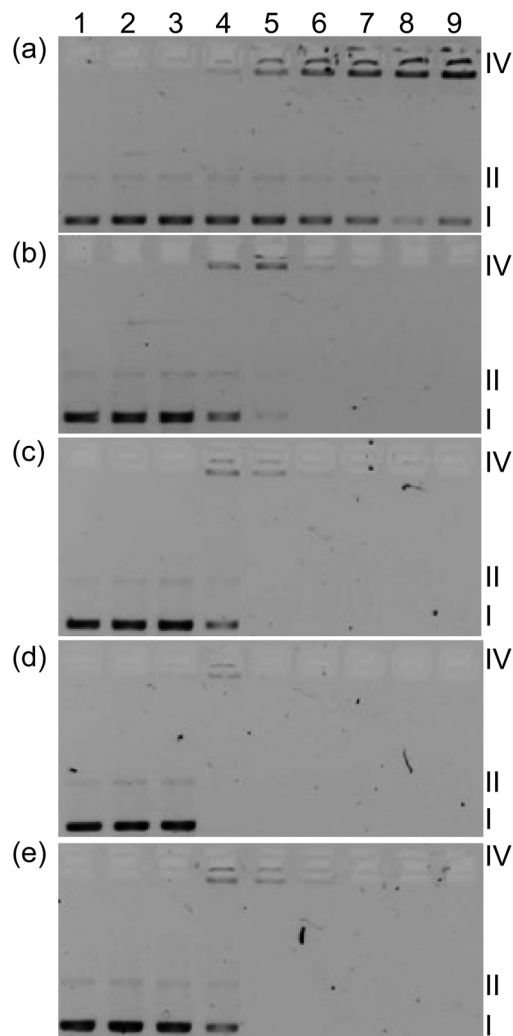


Fig. 7 DNA photocleavage of pUC19 DNA (20 μM bases) dosed with metal complex (MC) 1 (a), 2 (b), 3 (c), 4 (d) or 5 (e) and visible light (14 J cm^{-2}). Gel mobility shift assays employed 1% agarose gels (0.75 $\mu\text{g mL}^{-1}$ ethidium bromide) electrophoresed in 1 \times TAE at 8 V cm^{-1} for 30 min. Lane 1, DNA only ($-h\nu$); lane 2, DNA only ($+h\nu$); lane 3, 5 μM MC ($+h\nu$); lane 4, 20 μM MC ($+h\nu$); lane 5, 40 μM MC ($+h\nu$); lane 6, 60 μM MC ($+h\nu$); lane 7, 80 μM MC ($+h\nu$); lane 8, 100 μM MC ($+h\nu$); lane 9, 100 μM MC ($-h\nu$). Forms I, II, and IV DNA refer to supercoiled plasmid, nicked circular plasmid, and aggregated plasmid, respectively.

Conclusions

We have synthesized and characterized five heteroleptic cationic Ir(III) complexes with 2,3-diphenylbenzo[*g*]quinoxaline as the cyclometalating ligands and diimine ligands with varying degrees of π -conjugation as the coligand. The UV-vis absorption spectra of these complexes exhibited intense absorption bands below 500 nm and spin-forbidden broad absorption bands between 600 nm and 800 nm ($\epsilon < 200 \text{ M}^{-1} \text{ cm}^{-1}$). The intensities of these bands generally increased as the diimine ligand π -conjugation increased. All of the complexes possessed weak but structured emission in the NIR region, which was attributed to a dpbq ligand centred $^3\pi, \pi^*$ state combined with

some $^3\text{ILCT}/^3\text{MLCT}/^3\text{LLCT}$ character (supported by DFT calculations). The nanosecond TA spectra of complexes 1–4 all resembled that of the $[\text{Ir}(\text{dpbq})_2\text{Cl}]_2$ dimer, but the TA spectrum of complex 5 possessed features characteristic of both the quqo coligand and the $[\text{Ir}(\text{dpbq})_2\text{Cl}]_2$ dimer and a bi-exponential decay.

The Ir(III) complexes of this study were biologically active, with some members (2 and 3) acting as selective chemotherapeutics toward melanoma cells and others acting as potent *in vitro* PDT agents. These activities were in the nanomolar regime with SFs as large as 40 and PIs of almost 275 (5). The intracellular biological target(s) and mechanism of action are unknown at this time, but all of the Ir(III) complexes induced aggregation of DNA and production of $^1\text{O}_2$ in cell-free experiments, and were taken up readily by melanoma cells. The inherent NIR phosphorescence of these complexes translated to a convenient diagnostic tool for viewing cellular uptake and distribution. The systematic variation of the coligand in this class of complexes proved very influential, with very large differences in the resulting cytotoxicity and photocytotoxicity profiles, despite not having comparable differences in DNA interactions, $^1\text{O}_2$ quantum yields, and cellular uptake. The anticancer potency and breadth of activity in this small subset warrant further study of this new class of Ir(III) complexes, especially considering their demonstrated potential as *in vitro* theranostic PDT agents.

Acknowledgements

W. Sun acknowledges financial support from the Army Research Laboratory (W911NF-14-2-0081) for the synthesis and photophysical studies of the complexes, and the support from the Argonne National Laboratory *via* User Proposal CNM 48389. Use of the Center for Nanoscale Materials was supported by the US Department of Energy, Office of Science, Office of Basic Energy Sciences, under Contract No. DE-AC02-06CH11357. The computational part of the work was supported by NSF (DMR-1411086 and CNS-1229316) to W. Sun and S. Kilina. S. A. McFarland acknowledges financial support from the Natural Sciences and Engineering Council of Canada (NSERC), the Canadian Institutes of Health Research (CIHR), the Canadian Foundation for Innovation (CFI), the Nova Scotia Research and Innovation Trust (NSRIT), Acadia University, and the University of North Carolina at Greensboro.

Notes and references

- 1 R. Bonnett, *Chemical Aspects of Photodynamic Therapy*, Gordon and Breach Science Publishers, 2000.
- 2 M. R. Hamblin and Y.-Y. Huang, *Handbook of Photomedicine*, Taylor & Francis, 2014.
- 3 P. Agostinis, K. Berg, K. A. Cengel, T. H. Foster, A. W. Girotti, S. O. Gollnick, S. M. Hahn, M. R. Hamblin, A. Juzeniene, D. Kessel, M. Korbelik, J. Moan, P. Mroz,

- D. Nowis, J. Piette, B. C. Wilson and J. Golab, *CA-Cancer J. Clin.*, 2011, **61**, 250–281.
- 4 E. C. Glazer, *Isr. J. Chem.*, 2013, **53**, 391–400.
- 5 J. D. Knoll and C. Turro, *Coord. Chem. Rev.*, 2015, **282–283**, 110–126.
- 6 C. Mari and G. Gasser, *Chim. Int. J. Chem.*, 2015, **69**, 176–181.
- 7 C. Mari, V. Pierroz, S. Ferrari and G. Gasser, *Chem. Sci.*, 2015, **6**, 2660–2686.
- 8 O. J. Stacey and S. J. A. Pope, *RSC Adv.*, 2013, **3**, 25550–25564.
- 9 M. Stephenson, C. Reichardt, M. Pinto, M. Wächter, T. Sainuddin, G. Shi, H. Yin, S. Monroe, E. Sampson, B. Dietzek and S. A. McFarland, *J. Phys. Chem. A*, 2014, **118**, 10507–10521.
- 10 P. Vaupel and A. Mayer, *Cancer Metastasis Rev.*, 2007, **26**, 225–239.
- 11 W. R. Wilson and M. P. Hay, *Nat. Rev. Cancer*, 2011, **11**, 393–410.
- 12 H. Yin, M. Stephenson, J. Gibson, E. Sampson, G. Shi, T. Sainuddin, S. Monroe and S. A. McFarland, *Inorg. Chem.*, 2014, **53**, 4548–4559.
- 13 T. Sainuddin, J. McCain, M. Pinto, H. Yin, J. Gibson, M. Hetu and S. A. McFarland, *Inorg. Chem.*, 2016, **55**, 83–95.
- 14 R. Lincoln, L. Kohler, S. Monroe, H. Yin, M. Stephenson, R. Zong, A. Chouai, C. Dorsey, R. Hennigar, R. P. Thummel and S. A. McFarland, *J. Am. Chem. Soc.*, 2013, **135**, 17161–17175.
- 15 C. Reichardt, M. Pinto, M. Wächter, M. Stephenson, S. Kupfer, T. Sainuddin, J. Guthmuller, S. A. McFarland and B. Dietzek, *J. Phys. Chem. A*, 2015, **119**, 3986–3994.
- 16 T. Sainuddin, M. Pinto, H. Yin, M. Hetu, J. Colpitts and S. A. McFarland, *J. Inorg. Biochem.*, 2016, **158**, 45–54.
- 17 W. E. Ford and M. A. J. Rodgers, *J. Phys. Chem.*, 1992, **96**, 2917–2920.
- 18 N. D. McClenaghan, Y. Leydet, B. Maubert, M. T. Indelli and S. Campagna, *Coord. Chem. Rev.*, 2005, **249**, 1336–1350.
- 19 Y. Sun, L. E. Joyce, N. M. Dickson and C. Turro, *Chem. Commun.*, 2010, **46**, 2426–2428.
- 20 H. Xu, R. Chen, Q. Sun, W. Lai, Q. Su, W. Huang and X. Liu, *Chem. Soc. Rev.*, 2014, **43**, 3259–3302.
- 21 X. Yang, G. Zhou and W.-Y. Wong, *Chem. Soc. Rev.*, 2015, **44**, 8484–8575.
- 22 R. D. Costa, E. Ortí, H. J. Bolink, F. Monti, G. Accorsi and N. Armaroli, *Angew. Chem., Int. Ed.*, 2012, **51**, 8178–8211.
- 23 S. B. Meier, D. Tordera, A. Pertegás, C. Roldán-Carmona, E. Ortí and H. J. Bolink, *Mater. Today*, 2014, **17**, 217–223.
- 24 J. Zhao, W. Wu, J. Sun and S. Guo, *Chem. Soc. Rev.*, 2013, **42**, 5323–5351.
- 25 J. Zhou, Q. Liu, W. Feng, Y. Sun and F. Li, *Chem. Rev.*, 2015, **115**, 395–465.
- 26 C. K. Prier, D. A. Rankic and D. W. C. MacMillan, *Chem. Rev.*, 2013, **113**, 5322–5363.
- 27 S. Sato, T. Morikawa, T. Kajino and O. Ishitani, *Angew. Chem., Int. Ed.*, 2013, **52**, 988–992.
- 28 M. Feller, U. Gellrich, A. Anaby, Y. Diskin-Posner and D. Milstein, *J. Am. Chem. Soc.*, 2016, **138**, 6445–6454.
- 29 P. Majumdar, X. Yuan, S. Li, B. Le Guennic, J. Ma, C. Zhang, D. Jacquemin and J. Zhao, *J. Mater. Chem. B*, 2014, **2**, 2838–2854.
- 30 R.-R. Ye, C.-P. Tan, L. He, M.-H. Chen, L.-N. Ji and Z.-W. Mao, *Chem. Commun.*, 2014, **50**, 10945–10948.
- 31 L. He, Y. Li, C.-P. Tan, R.-R. Ye, M.-H. Chen, J.-J. Cao, L.-N. Ji and Z.-W. Mao, *Chem. Sci.*, 2015, **6**, 5409–5418.
- 32 A. Kando, Y. Hisamatsu, H. Ohwada, T. Itoh, S. Moromizato, M. Kohno and S. Aoki, *Inorg. Chem.*, 2015, **54**, 5342–5357.
- 33 M. Montalti, A. Credi, L. Prodi and M. T. Gandolfi, *Handbook of Photochemistry*, CRC Press, Taylor & Francis Group, LLC, Boca Raton, FL, 3rd edn, 2006, p. 620.
- 34 R. Gao, D. G. Ho, B. Hernandez, M. Selke, D. Murphy, P. I. Djurovich and M. E. Thompson, *J. Am. Chem. Soc.*, 2002, **124**, 14828–14829.
- 35 M. K. Nazeeruddin, R. Humphry-Baker, D. Berner, S. Rivier, L. Zuppiroli and M. Graetzel, *J. Am. Chem. Soc.*, 2003, **125**, 8790–8797.
- 36 C. Wang, L. Lystrom, H. Yin, M. Hetu, S. Kilina, S. A. McFarland and W. Sun, *Dalton Trans.*, 2016, **45**, 16366–16378.
- 37 Y. Choi, S. Kim, M.-H. Choi, S.-R. Ryoo, J. Park, D.-H. Min and B.-S. Kim, *Adv. Funct. Mater.*, 2014, **24**, 5781–5789.
- 38 V. Fernandez-Moreira, F. L. Thorp-Greenwood and M. P. Coogan, *Chem. Commun.*, 2010, **46**, 186–202.
- 39 Q. Zhao, M. Yu, L. Shi, S. Liu, C. Li, M. Shi, Z. Zhou, C. Huang and F. Li, *Organometallics*, 2010, **29**, 1085–1091.
- 40 G. Zhang, H. Zhang, Y. Gao, R. Tao, L. Xin, J. Yi, F. Li, W. Liu and J. Qiao, *Organometallics*, 2014, **33**, 61–68.
- 41 M. S. Lowry and S. Bernhard, *Chem. – Eur. J.*, 2006, **12**, 7970–7977.
- 42 K. Hasan, A. K. Bansal, I. D. W. Samuel, C. Roldán-Carmona, H. J. Bolink and E. Zysman-Colman, *Sci. Rep.*, 2015, **5**, 12325.
- 43 Ł. Skórka, M. Filapek, L. Zur, J. G. Małecki, W. Pisarski, M. Olejnik, W. Danikiewicz and S. Krompiec, *J. Phys. Chem. C*, 2016, **120**, 7284–7294.
- 44 R. Tao, J. Qiao, G. Zhang, L. Duan, L. Wang and Y. Qiu, *J. Phys. Chem. C*, 2012, **116**, 11658–11664.
- 45 R. Tao, J. Qiao, G. Zhang, L. Duan, C. Chen, L. Wang and Y. Qiu, *J. Mater. Chem. C*, 2013, **1**, 6446–6454.
- 46 L. Xin, J. Xue, G. Lei and J. Qiao, *RSC Adv.*, 2015, **5**, 42354–42361.
- 47 A.-H. Li, E. Ahmed, X. Chen, M. Cox, A. P. Crew, H.-Q. Dong, M. Jin, L. Ma, B. Panicker, K. W. Siu, A. G. Steinig, K. M. Stolz, P. A. R. Tavares, B. Volk, Q. Weng, D. Werner and M. J. Mulvihill, *Org. Biomol. Chem.*, 2007, **5**, 61–64.
- 48 M. Yu, Q. Zhao, L. Shi, F. Li, Z. Zhou, H. Yang, T. Yi and C. Huang, *Chem. Commun.*, 2008, 2115–2117.
- 49 H.-Y. Chen, C.-H. Yang, Y. Chi, Y.-M. Cheng, Y.-S. Yeh, P.-T. Chou, H.-Y. Hsieh, C.-S. Liu, S.-M. Peng and G.-H. Lee, *Can. J. Chem.*, 2006, **84**, 309–318.

- 50 N. Matsuo, *Bull. Chem. Soc. Jpn.*, 1974, **47**, 767–768.
- 51 O. E. Semonin, J. C. Johnson, J. M. Luther, A. G. Midgett, A. J. Nozik and M. C. Beard, *J. Phys. Chem. Lett.*, 2010, **1**, 2445–2450.
- 52 M. C. DeRosa and R. J. Crutchley, *Coord. Chem. Rev.*, 2002, **233–234**, 351–371.
- 53 M. J. Frisch, G. W. Trucks, H. B. Schlegel, G. E. Scuseria, M. A. Robb, J. R. Cheeseman, G. Scalmani, V. Barone, B. Mennucci, G. A. Petersson, H. Nakatsuji, M. Caricato, X. Li, H. P. Hratchian, A. F. Izmaylov, J. Bloino, G. Zheng, J. L. Sonnenberg, M. Hada, M. Ehara, K. Toyota, R. Fukuda, J. Hasegawa, M. Ishida, T. Nakajima, Y. Honda, O. Kitao, H. Nakai, T. Vreven Jr., J. A. Montgomery, J. E. Peralta, F. Ogliaro, M. Bearpark, J. J. Heyd, E. Brothers, K. N. Kudin, V. N. Staroverov, R. Kobayashi, J. Normand, K. Raghavachari, A. Rendell, J. C. Burant, S. S. Iyengar, J. Tomasi, M. Cossi, N. Rega, N. J. Millam, M. Klene, J. E. Knox, J. B. Cross, V. Bakken, C. Adamo, J. Jaramillo, R. Gomperts, R. E. Stratmann, O. Yazyev, A. J. Austin, R. Cammi, C. Pomelli, J. W. Ochterski, R. L. Martin, K. Morokuma, V. G. Zakrzewski, G. A. Voth, P. Salvador, J. J. Dannenberg, S. Dapprich, A. D. Daniels, Ö. Farkas, J. B. Foresman, J. V. Ortiz, J. Cioslowski and D. J. Fox, *Gaussian 09, Revision A.1*, Gaussian Inc., Wallingford, CT, USA, 2009.
- 54 E. K. U. Gross and W. Kohn, *Phys. Rev. Lett.*, 1985, **55**, 2850–2852.
- 55 M. E. Casida, in *Recent Advances in Computational Chemistry: Vol. 1 Recent Advances in Density Functional Methods*, ed. D. P. Chong, 1995, pp. 155–192.
- 56 L. Künnle, *Z. Phys. Chem.*, 1998, **204**, 263–264.
- 57 R. Bauernschmitt and R. Ahlrichs, *Chem. Phys. Lett.*, 1996, **256**, 454–464.
- 58 E. R. Davidson, *J. Comput. Phys.*, 1975, **17**, 87–94.
- 59 S. J. A. van Gisbergen, J. G. Snijders and E. J. Baerends, *Comput. Phys. Commun.*, 1999, **118**, 119–138.
- 60 J. P. Perdew, K. Burke and M. Ernzerhof, *Phys. Rev. Lett.*, 1996, **77**, 3865–3868.
- 61 V. Barone and M. Cossi, *J. Phys. Chem. A*, 1998, **102**, 1995–2001.
- 62 R. L. Martin, *J. Chem. Phys.*, 2003, **118**, 4775–4777.
- 63 A. Klamt and G. Schuurmann, *J. Chem. Soc., Perkin Trans. 2*, 1993, 799–805.
- 64 D. M. York and M. Karplus, *J. Phys. Chem. A*, 1999, **103**, 11060–11079.
- 65 E. R. Batista and R. L. Martin, *Encyclopedia of Computational Chemistry*, John Wiley and Sons Ltd., Chichester, U.K., 2004.
- 66 G. A. Zhurko and D. A. Zhurko, *ChemCraft 1.7*, <http://www.chemcraftprog.com>.
- 67 Z. Li, P. Cui, C. Wang, S. Kilina and W. Sun, *J. Phys. Chem. C*, 2014, **118**, 28764–28775.
- 68 L. Wang, P. Cui, S. Kilina and W. Sun, *J. Phys. Chem. C*, 2017, **121**, 5719–5730.
- 69 E. E. Langdon-Jones, A. J. Hallett, J. D. Routledge, D. A. Crole, B. D. Ward, J. A. Platts and S. J. A. Pope, *Inorg. Chem.*, 2013, **52**, 448–456.
- 70 W. Sun, C. Pei, T. Lu, P. Cui, Z. Li, C. McCleese, Y. Fang, S. Kilina, Y. Song and C. Burda, *J. Mater. Chem. C*, 2016, **4**, 5059–5072.
- 71 R. Liu, N. Dandu, J. Chen, Y. Li, Z. Li, S. Liu, C. Wang, S. Kilina, B. Kohler and W. Sun, *J. Phys. Chem. C*, 2014, **118**, 23233–23246.
- 72 E. M. Kober, J. V. Caspar, R. S. Lumpkin and T. J. Meyer, *J. Phys. Chem.*, 1986, **90**, 3722–3734.
- 73 L. Della Ciana, W. J. Dressick, D. Sandrini, M. Maestri and M. Ciano, *Inorg. Chem.*, 1990, **29**, 2792–2798.
- 74 R. Kumar, T. Y. Ohulchanskyy, I. Roy, S. K. Gupta, C. Borek, M. E. Thompson and P. N. Prasad, *ACS Appl. Mater. Interfaces*, 2009, **1**, 1474–1481.
- 75 S.-H. Wu, J.-W. Ling, S.-H. Lai, M.-J. Huang, C. H. Cheng and I.-C. Chen, *J. Phys. Chem. A*, 2010, **114**, 10339–10344.
- 76 E. C. Glazer, D. Magde and Y. Tor, *J. Am. Chem. Soc.*, 2005, **127**, 4190–4192.
- 77 E. Sakuda, C. Matsumoto, Y. Ando, A. Ito, K. Mochida, A. Nakagawa and N. Kitamura, *Inorg. Chem.*, 2015, **54**, 3245–3252.
- 78 K. A. King and R. J. Watts, *J. Am. Chem. Soc.*, 1987, **109**, 1589–1590.
- 79 A. P. Wilde, K. A. King and R. J. Watts, *J. Phys. Chem.*, 1991, **95**, 629–634.
- 80 S. Ladouceur, L. Donato, M. Romain, B. P. Mudraboyina, M. B. Johansen, J. A. Wisner and E. Zysman-Colman, *Dalton Trans.*, 2013, **42**, 8838–8847.
- 81 K. Y. Zhang, H.-W. Liu, M.-C. Tang, A. W.-T. Choi, N. Zhu, X.-G. Wei, K.-C. Lau and K. K.-W. Lo, *Inorg. Chem.*, 2015, **54**, 6582–6593.
- 82 Y.-S. Yeh, Y.-M. Cheng, P.-T. Chou, G.-H. Lee, C.-H. Yang, Y. Chi, C.-F. Shu and C.-H. Wang, *ChemPhysChem*, 2006, **7**, 2294–2297.
- 83 Z. Li, H. Li, B. J. Gifford, W. D. N. Peiris, S. Kilina and W. Sun, *RSC Adv.*, 2016, **6**, 41214–41228.
- 84 D. I. Praseuth, A. Gaudemer, J.-B. Verlhac, I. Kraljic, I. Sissoëff and E. Guillé, *Photochem. Photobiol.*, 1986, **44**, 717–724.
- 85 D. T. Croke, L. Perrouault, M. A. Sari, J. P. Battioni, D. Mansuy, C. Helene and T. Le Doan, *J. Photochem. Photobiol.*, 1993, **18**, 41–50.
- 86 E. R. Blazek, J. G. Peak and M. J. Peak, *Photochem. Photobiol.*, 1989, **49**, 607–613.